Environment Protection Engineering

Vol. 48 2022 No. 1

DOI: 10.37190/epe220101

KAVIYA PIRIYAH SUNDAR (ORCID: 0000-0003-2728-2434)[1], SELLAPPA KANMANI

DESIGN OF UVA-LED CONCENTRIC GLASS TUBE MICROREACTOR AND EVALUATION OF PHOTOCATALYSIS WITH SIMULTANEOUS ADSORPTION AND HYDRODYNAMIC CAVITATION FOR FLUORESCENT DYE DEGRADATION

A slurry UVA-LED concentric glass tube reactor (CGTR) with micro-depthof 2 mm was designed for plug flow behaviour (length/effective diameter = 150). The reactor design considered uniform radial concentration and hydrodynamic cavitation. The 100% Acridine Orange dye (3.77×10^{-5} M) was removed within 35 min at the graphene oxide dose of 0.3 g/dm^3 and initial pH 11. It was observed that hydrodynamic cavitation shortened the reaction time and enhanced the apparent reaction rate constant from 0.022 to 0.109 min^{-1}. Further, the degradation pathway showed that decolourized dye solution consisted of ethylenedione (34%), indicating the oxidative reaction occurred.

1. INTRODUCTION

Photocatalysis has widespread applications such as synthesis of pharmaceutical ingredients, water splitting, self-cleaning applications and environmental applications including water/wastewater/air/soil purification [1]. Concerning dye degradation studies, fluorescent dyes when released into water resources cause mutagenic effects when they bind with DNA [2]. Fluorescent dyes contain fluorophores, which are similar to chromophores in reactive dyes. However, fluorophores absorb UV and visible radiation and emit light of a smaller wavelength since the part of energy absorbed is relaxed internally through radiationless vibration [3]. Acridine Orange (AO) is one of the heterocyclic fluorescent dyes containing nitrogen atoms. Acridines are widely used in dyeing, printing, lithography and biological applications as stains. These dyes are difficult to degrade when compared to reactive dyes due to their stability of combined aromatic planar cyclic

[1]Centre for Environmental Studies, Anna University, Guindy, Chennai – 600025, India, corresponding author K. P. Sundar, email address: kaviya1305@gmail.com

molecules with several π bonds. Conventional processes like chemical oxidation, coagulation, biological degradation are insufficient to mineralize these recalcitrants. Heterogeneous photocatalysis seems to be an environmentally sound technology successful in the degradation of the recalcitrant organics.

The common challenge in heterogeneous photocatalysis is the designing of a feasible photocatalytic reactor balancing various factors including uniform light irradiation, throughput and performance. Designs of various photocatalytic reactors have been developed [4]. The number of immobilized reactors and their variants are comparatively more researched than the slurry reactors. This may be due to the difficulty in photocatalyst separation at the end of the treatment.

The performance of the process mainly depends on photon and mass transfer efficiencies. There is a timescale difference between photon-catalyst surface interactions (~μs) and catalyst-substrate interactions (~s) [5]. Efficient designing of photocatalytic reactor systems can solve this problem. When considering mass transfer limitations, slurry photocatalyst systems work better when compared to immobilized photocatalyst systems [6]. In slurry photocatalysts, the reacting surface of the catalyst is available more to the substrate medium. Thus this reduces the timescale of catalyst-substrate interactions. On the other hand, the type and configuration of the light source are important to increase the photon transfer efficiency. The light source has evolved from conventional lamps to light-emitting diodes (LEDs) in the last three decades. The comparison of conventional lamps and LEDs showed that the latter light source consumed 5 times less energy than the former [7]. Also, the lifetime of LED is much longer of around 50 000 h, whereas Hg lamps have a lifetime of around 2000 h. Further several other advantages of LEDs are less heat generation, no mercury or other toxic gases, flexibility in design and degree of freedom [8].

Dye substances get easily adsorbed to carbonaceous materials [9, 10]. Graphene is a single layer of easily synthesised graphite that has a large surface area (~2600 m^2/g) [11]. Graphene has zero band-gap because the conduction and valence bands meet at the Dirac points. Further increasing the oxygen functionalities (O content 20–40%) to the graphene widens the band-gap making an excellent photocatalyst. Therefore graphene oxide was taken as a photocatalyst to have adsorption enhanced photocatalysis.

Hydrodynamic cavitation has been studied widely in the past decades, due to its energy efficiency and easy industrial scalability [12]. In hydrodynamic cavitation, bubbles are formed during passing the liquid through the in-line venturi, orifice or plate. When the pressure at the constriction falls below the vapour pressure of the liquid, there are numerous air bubbles formed, and that subsequently collapses downstream of pressure recovery. The collapse induces shock waves cleaving water molecules to generate reactive free radicals and enhances mass transport rates. These radicals oxidize the persistent organic pollutants. This can further enhance the rate of oxidation. Also, the generation of high-speed micro-jets and intensive shockwaves may be a possibility for the surface cleaning of catalyst active sites and enhancement in local mass transport rates [13].

In this article, a novel cylindrical concentric glass tube reactor (CGTR) is designed and developed. The main feature of the reactor is the micro-depth substrate, constricted reactor inlet, suspended catalyst nature and circumferential LED pattern. There was a combined process of adsorption, photocatalysis and hydrodynamic cavitation observed contributing to the higher efficiency than individual processes. The dye degradation pathway was proposed, which showed that the dye structure was oxidized within a short time due to synergism between the three processes.

2. MATERIALS AND METHODS

Reactor design. The photocatalytic reactor setup is shown in Fig. 1. The inlet reservoir contains 1 dm^3 of Acridine Orange (AO) ($3.77 \cdot 10^{-5}$ mol/dm^3). The molecular weight of AO is equal to 265.4 g/mol and the dye molecular formula can be expressed as $C_{17}H_{19}N_3$. The dye solution is transmitted to the UVA-LED CGTR using a submersible pump.

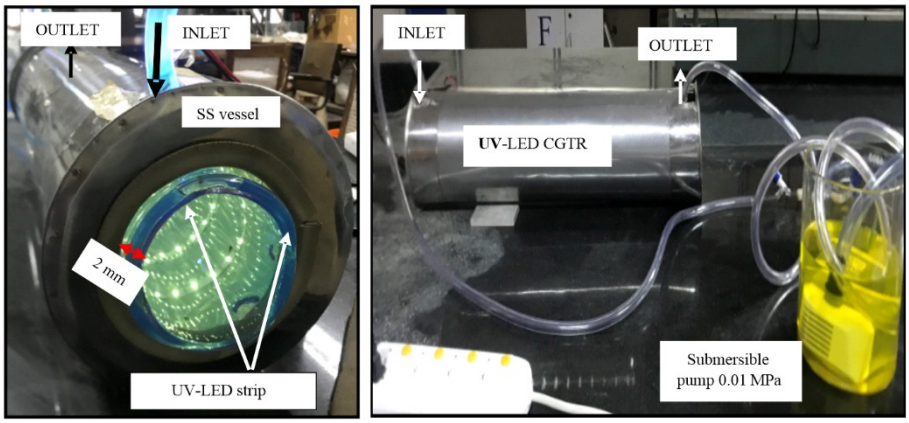

Fig. 1. UVA-LED CGTR setup

There is a constricted inlet in the reactor which leads to the pressure drop and formation of air bubbles downstream (Figs. 2 and 3). These cavities contribute to high turbulence enhancing photocatalyst-reactant interaction and formation of oxidation products. The reactor assembly consists of a cylindrical concentric glass tube 60 cm long and 8 cm in diameter fitted inside a stainless steel vessel 60 cm long and 14 cm in diameter. The lateral dimension of the concentric glass tube is 2 mm, which makes the light penetration uniform and there is another vessel inside to cover the opposite side of the glass. The substrate thickness would be 2 mm to produce micro-depth for an efficient photocatalytic reaction. The concentric glass tube is closed at both ends with appropriate

enclosures. The capacity of the reactor is 300 cm^3. The inlet flow is 2.25 dm^3/min and the inlet pressure of 0.01 MPa were measured using a pressure gauge. The cavitation number was calculated to be 0.9 according to the formula reported by Saharan et al. [13]. In the interior walls of a stainless steel vessel, the LED strip containing 300 numbers of UVA--LEDs (λ = 365 nm) is circumferentially placed for uniform irradiation (27 W/m^2). The distance between dye solution and LED is 3 cm. Ø

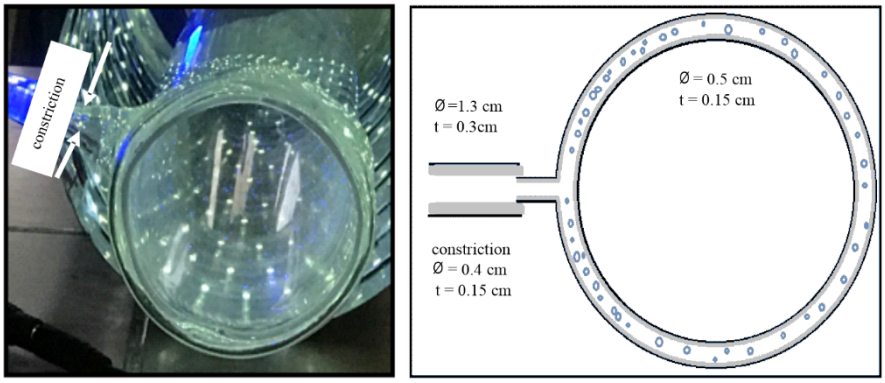

Fig. 2. Constricted geometry; ∅ – diameter, t – thickness)

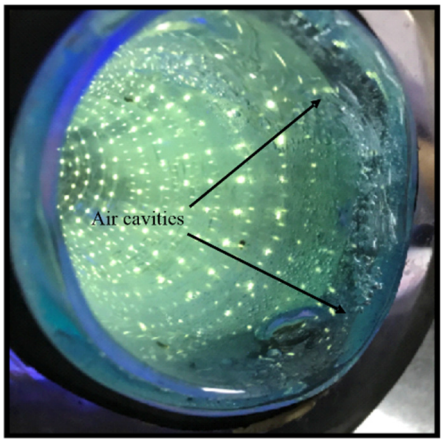

Fig. 3. Hydrodynamic cavitation at the inlet zone

Catalyst characterization. Catalyst graphene oxide (GO) was purchased at Nanowings Pvt. Ltd. (R&D Centre). The catalyst was characterized using scanning electron microscopy (SEM) with energy-dispersive X-ray spectroscopy (EDS) to study morphology and elemental composition (Tescan Vega). The crystal structure was determined using an X-ray diffractometer with CuKα radiation. Infrared spectra were obtained by a Fourier transform infrared spectrophotometer in the range between 500 and 3500 cm^{-1}. The band-

gap was evaluated using UV-Visible diffuse reflectance spectroscopy (JASCO V-650: A061861150).

Experimental procedure. The following experimental conditions were evaluated in this study: 1) dark adsorption, 2) photolysis, 3) hydrodynamic cavitation, 4) photocatalysis with initial adsorption (PCIA), 5) photocatalysis with initial adsorption and hydrodynamic cavitation (PCIA + HC), 6) photocatalysis with simultaneous adsorption (PCSA), and 7) photocatalysis with simultaneous adsorption and hydrodynamic cavitation (PCSA + HC). In photocatalysis with initial adsorption, 30 min of dark adsorption-desorption was attained before photocatalysis. Hydrodynamic cavitation was induced with the help of a submersible pump (inlet pressure 0.01 MPa) and constricted geometry (effective diameter 0.1 cm) at the inlet. In photocatalysis with simultaneous adsorption, the dye solution and catalyst graphene oxide particles were directly injected into the reactor without dark adsorption. The samples were collected at the outlet of the reactor and analyzed for absorbance with the use of a UV-Visible spectrophotometer at wavelength 489 nm for every 5–10 min time interval. The colour removal was calculated using an equation:

$$\text{Colour removal} = \frac{A_0 - A}{A_0}$$

where A_0 and A are the initial and final absorbances of the dye solution. Catalyst dosage (0.1–0.5 g/dm^3) and initial pH (4–12) were varied and optimized conditions for maximum colour removal were obtained for the developed CGTR.

Gas chromatography analysis was used to study the reaction intermediates and degradation pathways. The analysis required 0.05 cm^3 of the liquid sample which were dissolved in 1 cm^3 of GC grade ethyl acetate and mixed using a vortex mixer. Then the sample was filtered through a 0.45 μm filter cartridge and injected into the GC-MS instrument (Agilent Technologies 7890B).

In this study, comparison of kinetic behaviour between graphene oxide and Degussa P-25 TiO_2 was done, where 0.3 g/dm^3 catalyst dosage, initial pH 11 was chosen for the experiments.

3. RESULTS AND DISCUSSION

3.1. CATALYST CHARACTERIZATION

Figure 4 shows the morphology and composition of graphene oxide (GO); the width was about 10 μm. GO had an oxygen content of 34%. The atomic ratio of carbon to oxygen was 1.76. The X-ray diffraction spectra shown in Fig. 5 indicate characteristic

peaks were at 2θ of 20.53°; 22.9° and 26.57° which correlated with published XRD patterns of graphene oxide [14]. Multi-layered graphene oxide had a thickness of 5–20 nm and an average particle diameter of 1–10 µm. FTIR spectra (Fig. 6) of GO consist of carboxyl C=O stretching band at 1778 cm^{-1}, O–H deformation vibration band at 1396 cm^{-1} and C–O stretching vibration at 1069 cm^{-1} [15]. Figure 7 shows the absorption spectrum of graphene oxide. The bandgap was found out to be 3.1 eV, using the Tauc plot (Fig. 8).

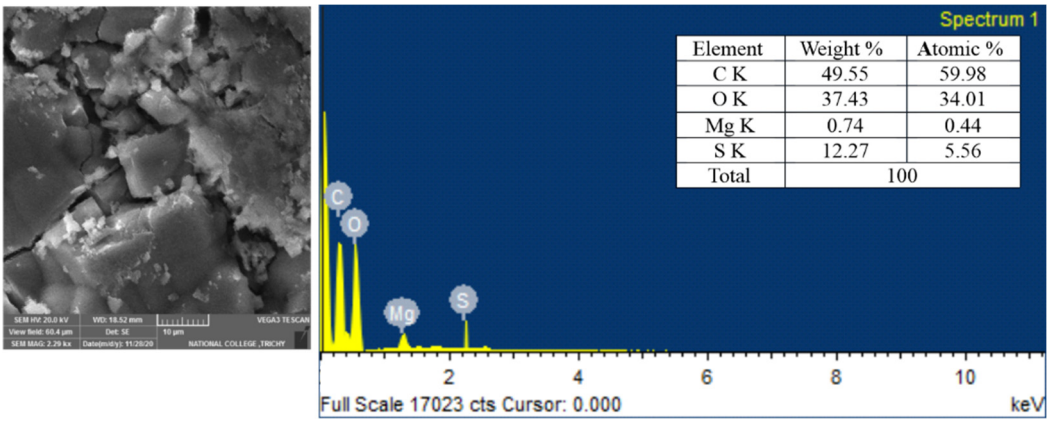

Fig. 4. SEM and EDX of graphene oxide

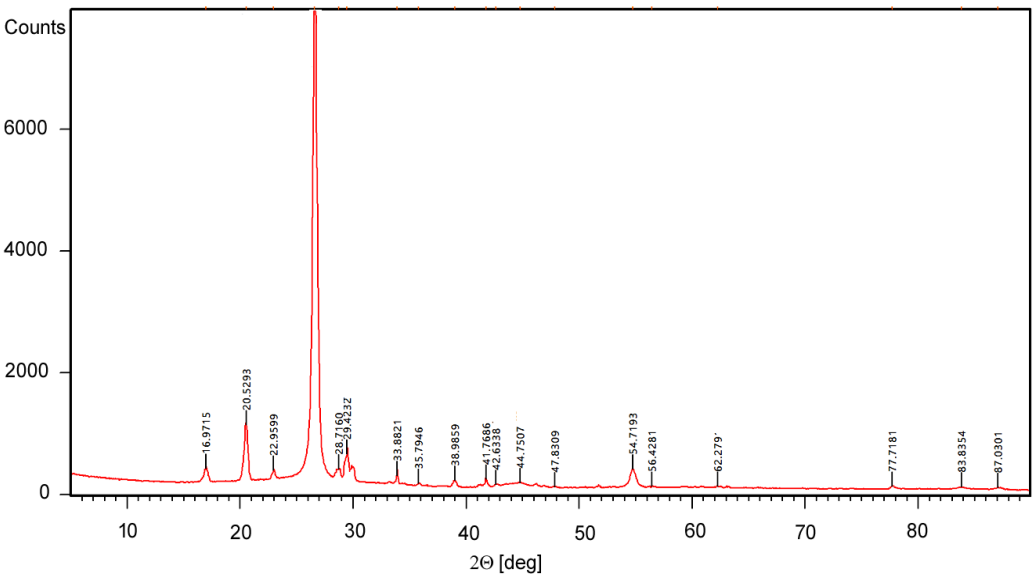

Fig. 5. XRD pattern of graphene oxide

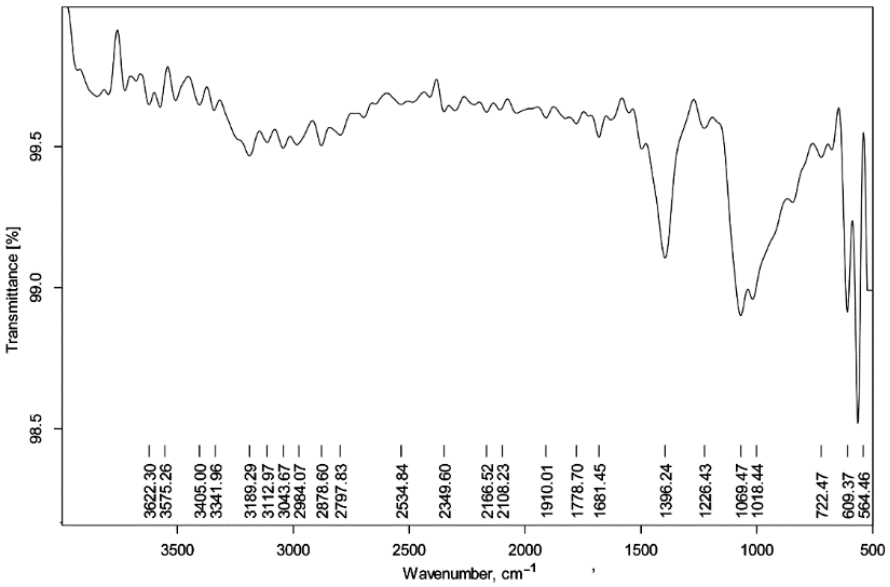

Fig. 6. FTIR spectrum of graphene oxide

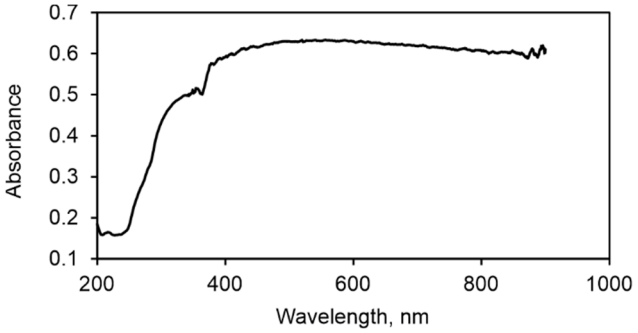

Fig. 7. UV-visible absorption spectra of graphene oxide

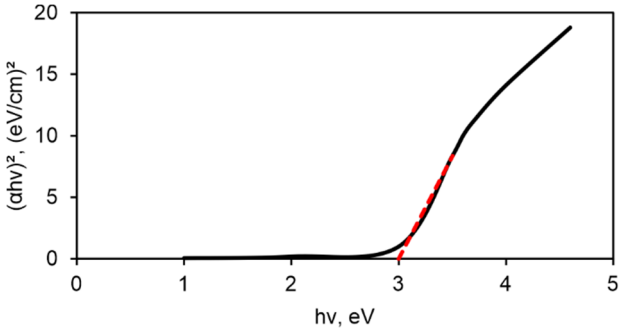

Fig. 8. Tauc plot for the bandgap evaluation

3.2. EFFICIENCY OF COLOUR REMOVAL USING CGTR

The efficiency of dark adsorption of AO on graphene oxide photocatalyst was observed to be 20.9% and 39% in 30 min at natural pH 7.5 and initial pH 11, respectively. The reason for dark adsorption was attributed to the presence of oxygen functional groups of graphene oxide. Under pure photolysis, the reactor was filled only with the dye solution under gravity flow (no hydrodynamic cavitation) and irradiated for 30 min. The colour removal amounted to 4.4% and 7.7% at natural pH 7.5 and initial pH 11, respectively. This implied that the excitation of dye molecules by photons had an insignificant effect on colour removal. Under hydrodynamic cavitation, dye solution was injected into the reactor using a submersible pump with no irradiation. It was observed that the colour was removed insignificantly (2–2.5%) at both natural pH 7.5 and initial pH 11.

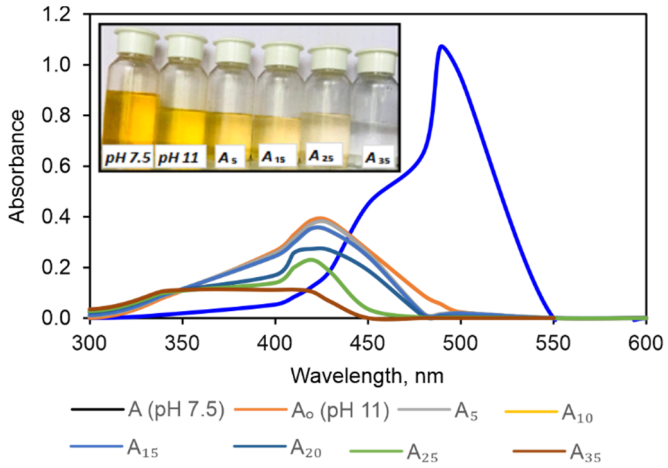

Fig. 9. Chemical quenching of AO: A – natural pH 7.5, A_0 – initial pH 11, A_5, A_{10}, A_{15}, A_{20}, A_{30}, A_{35} – 5, 10, 15, 20, 30, 35 min irradiated samples

pH is an important parameter in the photocatalysis of ionic structures like dye molecules. The AO dye shows a strong peak at 489 nm and a weak shoulder at 470 nm, which have similar correlations with literature data [16]. This was due to the existence of mono-protonated and di-protonated AO species. It was interesting to note that the absorption peak was shifted to 420 nm when the initial pH was adjusted to 11. Also, there was a decrease in colour intensity due to chemical quenching by hydroxyl anions. This may be because, under elevated pH (>10), the weak basic dye becomes mono-cationic (single proton on acridine nitrogen). This mono-cationic structure forms strong H-bonding with hydroxyl anions in the solution. Thus weakening the π bonds in the dye structure resulting in a decrease in colour intensity. As the dye gets degraded under

photocatalysis with simultaneous adsorption and hydrodynamic cavitation, the absorbance gradually decreased (Fig. 9). The pH effect on photocatalytic activity depends also on catalyst zero-point charge, the ionic form of dye and the dissociation constant of dye. Electrostatic attraction enhances the kinetics of the reaction, where the catalyst surface should possess a charge (positive or negative) countering the charge of dye molecules [17, 18]. Since AO dye molecules have amino groups cationic in nature, therefore in an alkaline medium, the graphene oxide surface might possess a negative charge. The zero point charge of graphene oxide is 2.134 [19]. At pH > 2.1, graphene oxide might be negatively charged. Further, the pK_a (isoelectric point) of AO is 9.6, thus for pH > 9.6 the dissociation of dye is enhanced, subsequently the adsorption onto the catalyst particles is improved [20].

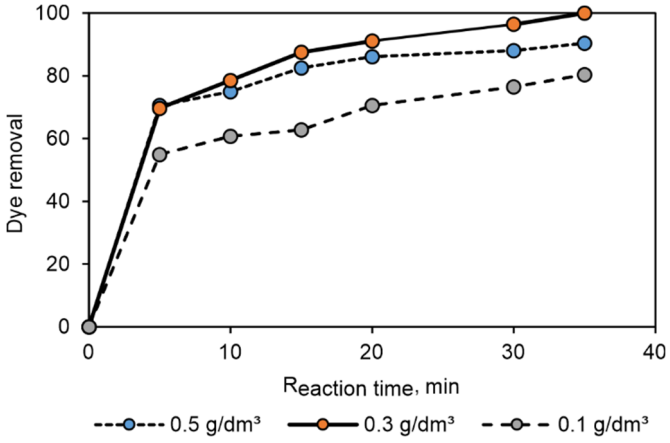

Fig. 10. Effect of catalyst dosage on colour removal (process PCSA + HC, initial pH 11)

The catalyst dosage was varied from 0.1 to 0.5 g/dm^3 at initial pH 11 for PCSA + HC (Fig. 10). It was observed that at the dosage of 0.1 g/dm^3, initial adsorption was predominant and rapid, then later there was a decrease in the rate of colour removal. This decrease may be attributed to insufficient catalyst dosage for the reaction. In the case of 0.5 g/dm^3 and 0.3 g/dm^3, there was similarity in initial adsorption till first 5 min, later the colour removal decreased in the case of 0.5 g/dm^3 may be due to inhibition of light penetration. Therefore it implied that optimum catalyst dosage (0.3 g/dm^3) was required to offer maximum photocatalytic active sites. Low catalyst dosage (0.1 g/dm^3) showed no significant photocatalytic activity, although the adsorption rate was faster. High catalyst dosage (0.5 g/dm^3) inhibited the light penetration depth and increased the electron-hole recombination centres [21].

Photocatalysis with initial adsorption (PCIA) was evaluated with different pH values as shown in Fig. 11. It was observed that there was a steady increase in % colour

removal with reaction time. This showed that the reaction followed pseudo-first order kinetics. At initial pH 11, the maximum colour removal was 39% in 60 min reaction time. When pH was increased to 12, the colour removal declined. On the other hand, the % colour removal decreased gradually when pH was decreased till the initial pH 4. This was since the pH influences the surface charge characteristics and the charge of organic molecules, which governs the adsorption capacity of molecules onto catalyst particles surface and the quantity of hydroxyl reactive radicals [22].

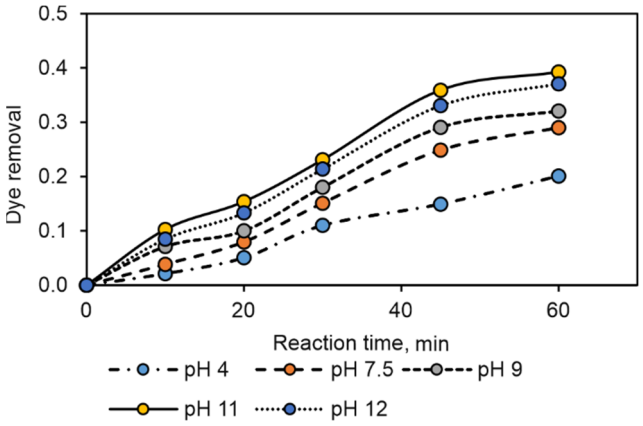

Fig. 11. The effect of pH on colour removal (process PCIA, catalyst dosage 0.3 g/dm^3)

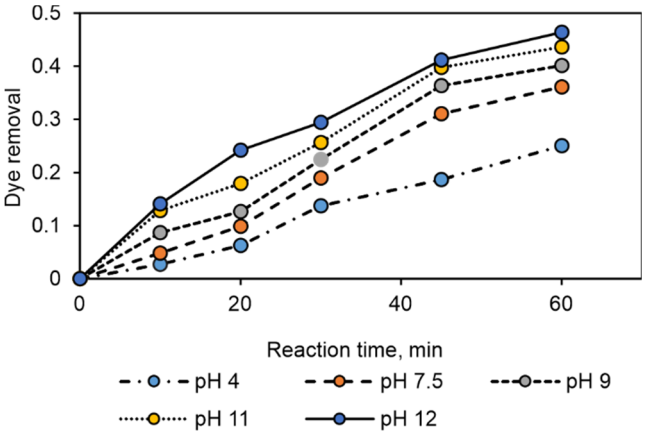

Fig. 12. The effect of pH on colour removal (process PCIA + HC, catalyst dosage 0.3 g/dm^3)

Similarly, photocatalysis with initial adsorption and hydrodynamic cavitation (PCIA + HC) was evaluated with different pH values as shown in Fig. 12. It was observed that the hydrodynamic cavitation increased the efficiency of the colour removal from 39%

(PCIA) to 43% (PCIA + HC) at initial pH 11. This may be due to the enhancement in mass transfer by turbulence and the availability of oxidizing radicals by the collapse of cavities. On average, the hydrodynamic cavitation increased the colour removal on a factor of 1.2 compared to PCIA for all pH values.

In the case of photocatalysis with simultaneous adsorption (PCSA), there was two-stage degradation observed (Fig. 13). In the first stage, adsorption was predominant till 30 min, although photocatalysis reaction takes place simultaneously. In the second stage of 30 min, the photocatalysis was steady and more dominant than adsorption. At initial pH 4, the colour removal was the lowest due to the low adsorption affinity between di- or tri-cationic acridine structures and protonated catalyst particles. At natural pH 7.5 and 9, there was moderate colour removal efficiency of up to 24–27%. At pH 11, there was 71% colour removal in first stage adsorption (30 min), followed by 80% colour removal in remaining 30 min of reaction time. The rapid adsorption might be due to increased attraction between mono-cationic acridine structures and hydroxylated catalyst particles. The electrostatic attraction increases the probability of photocatalytic degradation of AO under UVA irradiation.

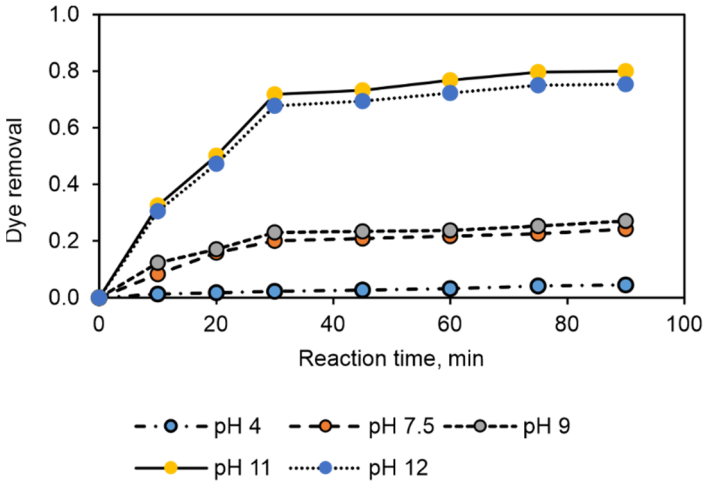

Fig. 13. The effect of pH on colour removal
(process PCSA, catalyst dosage 0.3 g/dm^3)

Similarly, photocatalysis with simultaneous adsorption and hydrodynamic cavitation (PCSA + HC) also consisted of two stages of dye degradation (Fig. 14). But PCSA + HC was quite faster and more efficient than PCSA due to mixing and cavitation. Hydrodynamic cavities are formed when liquid undergoes a dynamic pressure reduction due to constricted inlet geometry under constant temperature (according to Charles law). At the downstream, when the pressure recovers, the cavities collapse. Cavitation bubbles collapse induces mixing, homogenization and dispersion of solid–liquid system.

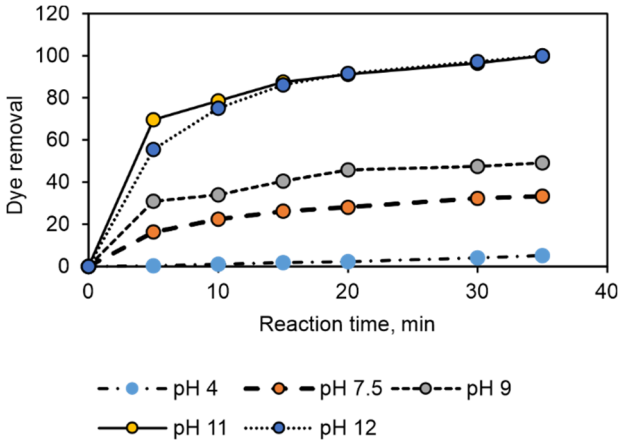

Fig. 14. The effect of pH on colour removal
(process PCSA + HC, catalyst dosage 0.3 g/dm^3)

The collapse of the cavities at the liquid–solid particles boundaries results in the dispersion of these catalyst particles in the fluid retaining the slurry nature of the photocatalytic system. Other than mechanical effects, the cavity collapse initiates physico-chemical effects initiating shock waves. These shock waves create extreme temperature and pressure dissociating H_2O molecules to $OH^{\bullet}$ and $H^{\bullet}$ radicals. At first 5 min, adsorption was predominant, then later photocatalysis was dominant till 35 min resulting in 100% colour removal. The observations revealed that synergism between pH adjustments, light irradiation, hydrodynamic cavitation, catalyst suspension and reactor geometry contributed to process intensification achieving complete colour removal. Similar works were carried out using Degussa P-25 TiO_2, which demonstrated that the combination of photocatalysis and hydrodynamic cavitation was twice better than individual processes in terms of pseudo-first-order rate constant [23].

3.3. PERFORMANCE ANALYSIS

The apparent reaction rate constants were calculated to compare the performance of the used CGTR under selected experimental conditions, i.e., photocatalysis with initial adsorption (PCIA), photocatalysis with initial adsorption and hydrodynamic cavitation (PCIA + HC), photocatalysis with simultaneous adsorption (PCSA) and photocatalysis with simultaneous adsorption and hydrodynamic cavitation (PCSA + HC). The plug flow model (PFR) was assumed for CGTR (length to effective diameter ratio is 150). Using the following equations, the reaction rate constant k for the PFR model can be calculated

$$-\frac{dC}{dt} = kC \tag{2}$$

$$-\ln\frac{C}{C_0} = kt \tag{3}$$

where k is the reaction rate constant at full surface coverage (min^{-1}), C is the dye concentration, C_0 is the initial dye concentration, and t is the reaction time (min).

For a combination of two treatment processes, the linearity is not obtained between $-\ln(C/C_0)$ and reaction time. Therefore two-stage degradation kinetic constants were derived by splitting the graphs. In the first stage, the reaction might be the adsorption dominant with reaction rate constant (K_1) and in the second stage, the reaction might be the photocatalysis dominant with reaction rate constant (K_2). The apparent reaction rate constant k_{app} was derived assuming a time-weighted average of K_1 and K_2

$$k_{app} = \frac{K_1 t_1 + K_2 t_2}{t_1 + t_2} \tag{4}$$

The apparent reaction rate constant was 0.009 min^{-1} for PCIA and PCIA + HC with the regression coefficient R^2 = 0.98. In PCSA and PCSA + HC cases, the first order reaction expression was not observed due to combined effects of adsorption, photocatalysis and hydrodynamic cavitation.

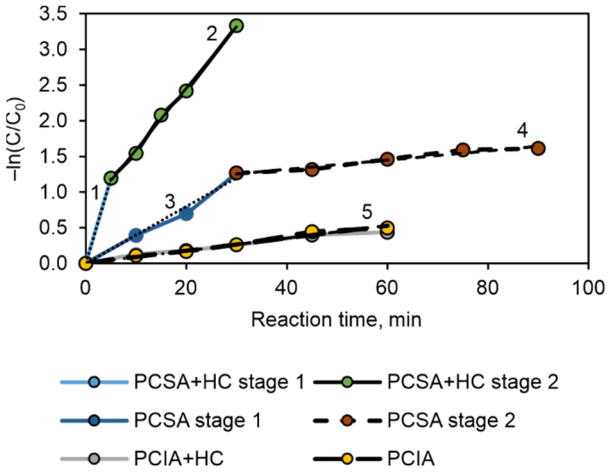

Fig. 15. Results of the kinetic study:
1) K_1 = 0.238, R^2 = 1, 2) K_2 = 0.088, R^2 = 0.99, 3) K_1' = 0.039, R^2 = 0.98, 4) K_2' = 0.0067, R^2 = 0.95, 5) k_3/k_4 = 0.009 min^{-1}, R^2 = 0.98, where K_1, K_2 – first and second stage reaction rate constants for PCSA + HC, K_1', K_2' – first and second stage reaction rate constant for PCSA, k_3, k_4 – reaction rate constants for PCIA + HC and PCIA, respectively; catalyst dosage 0.3 g/dm^3, initial pH 11

In Figure 15, the lines were split into two stages to calculate the stage-wise reaction rate constant (where R^2 is near 1). Therefore, the time-weighted apparent reaction rate constant was calculated for comparison. Table 1 shows the value of time-weighted apparent reaction rate constants for the selected experimental conditions.

Table 1. Reaction rate constants for 4 operating conditions

Condition type	k_{app} [min^{-1}]	t [min]
PCIA	0.009	60
PCIA + HC	0.009	60
PCSA	0.022	60
PCSA + HC	0.109	35

In the case of PCSA + HC, the slope line was steeper than observed for PCSA, due to mechanical and physicochemical effects intensifying the colour removal efficiency. For PCSA, the first-stage reaction rate (adsorption dominant) constant K_1 was 0.039 min^{-1} (R^2 = 0.98) and the second-stage reaction rate (photocatalysis dominant) constant K_2 was 0.006 min^{-1} (R^2 = 0.95). For PCSA + HC, the first-stage reaction rate (adsorption dominant) constant K_1' was 0.238 min^{-1} (R^2 = 1) and the second-stage reaction rate (photocatalysis dominant) constant K_2' was 0.088 min^{-1} (R^2 = 0.99). This implied that in the presence of hydrodynamic cavitation, the rate constants K_1 and K_2 increased 6 and 14.6 times, respectively.

3.4. COLOUR REMOVAL WITH GRAPHENE OXIDE GO AND DEGUSSA P-25 TiO_2

The optimized conditions (process PCSA + HC, catalyst dosage 0.3 g/dm^3 and initial pH 11) were evaluated with Degussa P-25 TiO_2 (thickness 0.5 nm and lateral size 1–10 μm) which resulted in 61.9% colour removal in 30 min of reaction time (k_{app} = 0.032 min^{-1}).

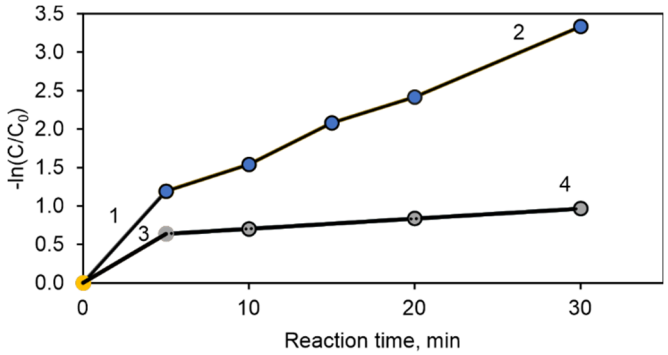

Fig. 16. Data for kinetics Degussa P25-TiO_2 and GO at 0.3 g/dm^3 catalyst dosage and intial pH 11
1) K_{1GO} = 0.238, R^2 = 0.99, 2) K_{2GO} = 0.088, R^2 = 0.99, 3) K_{1TiO_2} = 0.127, R^2 = 1, 4) K_{2TiO_2} = 0.013, R^2 = 0.99,
where K_{IGO}, K_{1TiO_2} – first and K_{2GO}, K_{2TiO_2} – second stage reaction rate constants
for PCSA + HC using GO and Degussa P25-TiO_2; catalyst dosage 0.3 g/dm^3, initial pH 11

The reaction rate constant was 3.4 times higher in the case of graphene oxide compared to Degussa P-25 (Fig. 16). This may be due to the point of zero charge value for

Degussa P-25 TiO_2 which is 6.5–7.5 as noted by several authors [24]. The higher pH value compared to that of graphene oxide implied that there was slow OH^- consumption of Degussa P-25 TiO_2 [25]. Therefore the electrostatic attraction between dye molecules and TiO_2 was comparatively less and slower, which made the photocatalytic degradation slower than graphene oxide.

3.5. DYE DEGRADATION PATHWAY

The intermediate products formed during AO colour removal by PCSA + HC process under optimized conditions (graphene oxide 0.3 g/dm^3 and initial pH 11) were iden-

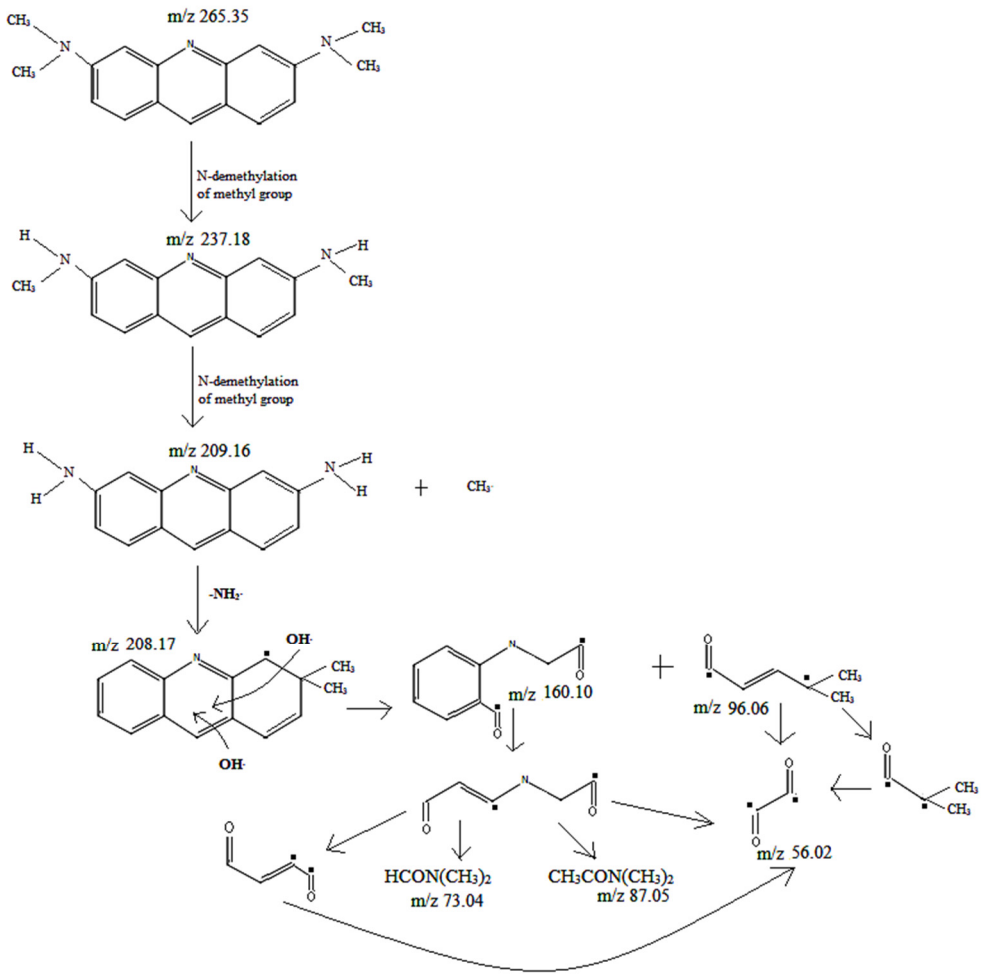

Fig. 17. Proposed degradation mechanism of AO
(PCSA + HC process, 0.3 g/dm^3 catalyst dosage initial pH 11)

tified using GC–MS results. The detected molecular weight of degraded organics molecules provides the degradation pathway of the dye and the proposed mechanism is presented in Fig. 17. The parent molecule AO, i.e., N,N,N′,N′-tetramethylacridine-3,6--diamine (*m*/*z* 265.2) was initially mono-protonated and forms high electrostatic bonding with graphene oxide at alkaline pH. The electrostatic attraction enhances the mass transfer between catalyst and dye molecules. When photo-generated hydroxyl radicals attacked the AO, N-demethylation occurred resulting in the N,N,N′,N′-de-tetramethyl acridine orange (*m*/*z* 209.16) [30]. Further, the amines were removed with the formation of 3,3-dimethyl acridine (*m*/*z* 208.17) and the ring structure was cleaved in the formation of 2-(carboxymethylamino) benzoic acid (*m*/*z* 160.1) and 4-methyl-2-pentenoic acid (*m*/*z* 96.06). These compounds got cleaved to form unstable organic radicals, which resulted in the formation of ethylene dione (*m*/*z* 56.02), N,N′-dimethyl acetamide (*m*/*z* 87.05), tertiary amide (*m*/*z* 73.04). The quantitative compositions were evaluated by the ratio of area under the peak for an individual compound and total area (Fig. 18).

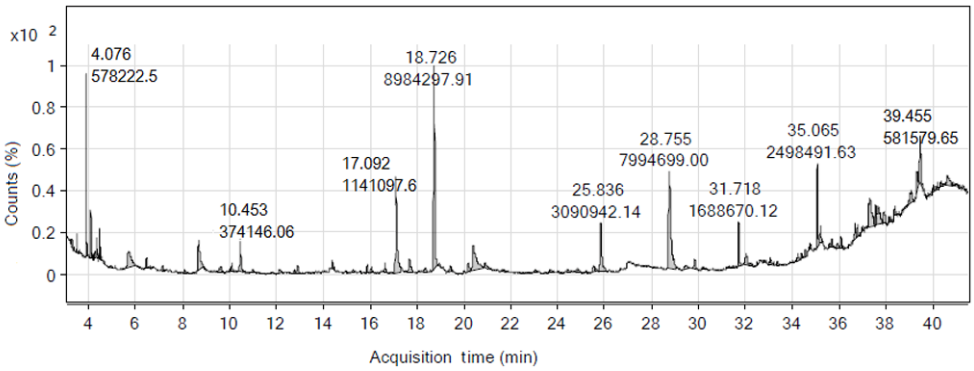

Fig. 18. GC-MS obtained for 35 min degraded AO solution
(PCSA + HC process, 0.3 g/dm^3 catalyst dosage, initial pH 11)

There was 34% of ethylenedione (18.73 min), 30% of 2-(carboxymethylamino) benzoic acid (28.75 min), 11% of 4-methyl-2-pentenoic acid (25.84 min), 9% of N, N′--de-dimethyl acridine orange (35.01 min), 6% of N,N,N′N′-de-tetramethyl acridine orange (31.72 min), 4% of N, N′-dimethyl acetamide (17.01 min) and 2% each of tertiary amide (4.08 min) and 2% of AO (39.455 min) present in the PCSA + HC treated solution under optimized conditions.

4. CONCLUSIONS

A photocatalytic reactor with a suspended catalyst system was designed for the micro-depth substrate. The length/diameter ratio for CGTR was 150, which incorporated the radial uniformity of reactant concentration. Through the constructed pathway in the

inlet zone, cavitation bubbles were formed. Further, the catalyst and pH-adjusted dye solution was injected into the reactor without dark adsorption, unlike the typical photocatalytic study. The AO colour intensity was decreased due to chemical quenching at the alkaline pH. Then the catalyst and dye molecules rapidly got attracted due to the electrostatic attraction and dye molecules got mineralized, which was shown in the degradation mechanism. The complex structure of AO dye (*m*/*z* 265.2) was broken to various intermediates such as N,N′ -de-dimethyl acridine orange, N,N, N′,N′-de-tetramethyl acridine orange, 3,3-dimethyl acridine, 2-(carboxymethylamino)benzoic acid and 4-methyl--2-pentenoic acid. Final step of oxidat021ion gives ethylenedione (*m*/*z* 56.02), N,N′--dimethyl acetamide (*m*/*z* 87.05) and tertiary amide (*m*/*z* 73.04). Although 80% dye was removed within 60 min in photocatalysis with simultaneous adsorption (PCSA), hydrodynamic cavitation accelerated the reaction by achieving 100% colour removal within 35 min. Hydrodynamic cavitation enhanced the rate of reaction by mixing, homogenization and hydroxyl production. Therefore, it was implicated that hybrid processes were more efficient when compared to individual processes.

ACKNOWLEDGEMENT

The authors acknowledge the Department of Science and Technology, Government of India for funding the research under DST INSPIRE fellowship (INSPIRE Code IF180373).

REFERENCES

[1] FUJISHIMA A., RAO T.N., TRYK D.A., *Titanium dioxide photocatalysis*, J. Photochem. Photobiol. C: Photochem. Rev., 2000, 1, 1–21. DOI: 10.1016/S1389-5567 (00)00002-2.

[2] ULLMANN F., *Triarylmethane and Diarylmethane Dyes*, *Ullmann's Encyclopedia of Industrial Chemistry*, 6th Ed., Wiley, New York 2001. DOI: 10.1002/14356007.a27_179.

[3] IARC Working Group on the Evaluation of Carcinogenic Risk to Humans, *Some Aromatic Amines, Organic Dyes, and Related Exposures*. *General Introduction to the chemistry of dyes*, Lyon 2010. DOI: https://www.ncbi.nlm.nih.gov/books/NBK385442/.

[4] SUNDAR K.P., KANMANI S., *Progression of photocatalytic reactors and its comparison*, Chem. Eng. Res. Des., 2020, 154, 135–150. DOI: 10.1016/j.cherd.2019.11.035.

[5] TURCHI S.C., OLLIS F.D., *Photocatalytic degradation of organic water contaminants: Mechanisms involving hydroxyl radical attack*, J. Catal., 1990, 122 (1), 178–192. DOI: 10.1016/0021-9517 (90)90269-P.

[6] MANASSERO A., SATUF M.L., ALFANO O.M., *Photocatalytic reactors with suspended and immobilized TiO_2. Comparative efficiency evaluation*, Chem. Eng. J., 2017, 326, 29–36. DOI: 10.1016/j.cej. 2017.05.087.

[7] KHADEMALRASOOL M., FARBOD M., TALEBZADEH M.D., *The improvement of photocatalytic processes: Design of a photoreactor using high-power LEDs*, J. Sci.-Adv. Mater. Dev., 2016, 1 (3), 382–387. DOI: 10.1016/j.jsamd.2016.06.012.

[8] BO-SEN W., HITTI Y., MACPHERSON S., ORSAT V., LEFSRUD M.G., *Comparison and perspective of conventional and LED lighting for photobiology and industry applications*, Environ. Exp. Bot., 2019, 171, 103953. DOI: 10.1016/j.envexpbot.2019.103953.

[9] LI Y., DU Q., LIU T., PENG X., WANG J., SUN J., WANG Y., WU S., WANG Z., XIA Y., XIA L., *Comparative study of methylene blue dye adsorption onto activated carbon, graphene oxide, and carbon nanotubes*, Chem. Eng. Res. Des., 2013, 91 (2), 361–368. DOI: 10.1016/j.cherd.2012.07.007.

[10] NGUYEN-PHAN T.-D., PHAM V.H., SHIN E.W., PAHM H.-D., KIM S., CHUNG J.S., *The role of graphene oxide content on the adsorption-enhanced photocatalysis of titanium dioxide/graphene oxide composites*, Chem. Eng. J., 2011, 170, 226–232. DOI: 10.1016/j.cej.2011.03.060.

[11] LI X., YU J., WAGEH S., AL-GHAMDI A.A., XIE J., *Graphene in photocatalysis: A review*, Small, 2016, 12 (48), 6640–6696. DOI: 10.1002/smll.201600382.

[12] SIVAKUMAR M., PANDIT A.B., *Wastewater treatment. A novel energy efficient hydrodynamic cavitational technique*, Ultrason. Sonochem., 2002, 9, 123–131. DOI: 10.1016/S1350-4177(01)00122-5.

[13] SAHARAN V.K., BADVE M.P., PANDIT A.B., *Degradation of Reactive Red 120 dye using hydrodynamic cavitation*, Chem. Eng. J., 2011, 178, 100–107. DOI: 10.1016/j.cej.2011.10.018.

[14] SIBURIAN R., SIHOTANG H., LUMBAN RAJA S., SUPENO M., SIMANJUNTAK C., *New route to synthesize of graphene nanosheets*, Orient. J. of Chem., 2018, 34 (1), 182–187. DOI: 10.13005/ojc/340120.

[15] CIPLAK Z., YILDIZ N., CALIMLI A., *Investigation of Graphene/Ag Nanocomposites Synthesis Parameters for Two Different Synthesis Methods*, Fuller. Nanotub. Carbon Nanostructures, 2014, 23, 361–370. DOI: 10.1080/1536383X.2014.894025.

[16] BHATTACHARJEE J., HUSSAIN S.A., BHATTACHARJEE D., *Control of H-dimer formation of acridine orange using nano clay platelets*, Spectrochim. Acta A Mol. Biomol. Spectrosc., 2013, 116, 148–153. DOI: 10.1016/j.saa.2013.07.018.

[17] LU C.S., MAI F.D., WU C.D., WU R.J., CHEN C., *Titanium dioxide-mediated photocatalytic degradation of Acridine Orange in aqueous suspensions under UV irradiation*, Dyes and Pigments, 2008, 76, 706–713. DOI: 10.1016/j.dyepig.2007.01.009.

[18] SOHRABI M.R., GHAVAMI M., *Photocatalytic degradation of Direct Red 23 dye using UV/TiO2. Effect of operational parameters*, J. Hazard. Mater., 2008, 153 (3), 1235–1239. DOI: 10.1016/j.jhazmat.2007.09.114.

[19] MONDAL N.K., CHAKRABORTY S., *Adsorption of Cr(VI) from aqueous solution on graphene oxide (GO) prepared from graphite: equilibrium, kinetic and thermodynamic studies*, Appl. Water Sci., 2020, 10 (61), 1–10. DOI: 10.1007/s13201-020-1142-2.

[20] QAMAR M., *Photodegradation of acridine orange catalyzed by nanostructured titanium dioxide modified with platinum and silver metals*, Desalin., 2010, 254 (1–3), 108–113. DOI: 10.1016/j.desal.2009.12.006.

[21] GHOLAMI M., SHIRZAD-SIBONI M., FARZADKIA M., YANG J.-K., *Synthesis, characterization, and application of ZnO/TiO$_2$ nanocomposite for photocatalysis of a herbicide (Bentazon)*, Desalin. Water Treat., 2015, 57 (29), 13632–13644. DOI: 10.1080/19443994.2015.1060541.

[22] AZEEZ F., AL-HETLANI E., ARAFA M., ABDELMONEM Y., NAZEER A.A., AMIN M.O., MADKOUR M., *The effect of surface charge on photocatalytic degradation of methylene blue dye using chargeable titania nanoparticles*, Scientific Reports, 2018, 8, 7104. DOI: https://www.nature.com/articles/s41598-018-25673-5.

[23] WANG X., JIA J., WANG Y., *Combination of photocatalysis with hydrodynamic cavitation for degradation of tetracycline*, Chemical Engineering Journal, 2017, 315, 274–282. DOI: 10.1016/j.cej.2017.01.011.

[24] LU C.-S., MAI F.-D., WU C.-W., WU R.-J., CHEN C.-C., *Titanium dioxide-mediated photocatalytic degradation of Acridine Orange in aqueous suspensions under UV irradiation*, Dyes and Pigments, 2008, 76, 706–713. DOI: 10.1016/j.dyepig.2007.01.009.

[25] FERNANDEZ-NIEVES A., RICHTER C., DE LAS NIEVES F.J., *Point of zero charge estimation for a TiO$_2$ /water interface*, Progress in Colloid and Polymer Science, 1998, 110, 21–24. DOI: /10.1007 %2FBFb0118041.